



Dopamine modulates the functional organization of the orbitofrontal cortex

Kahnt, Thorsten ; Tobler, Philippe N

Abstract: Neuromodulators such as dopamine can alter the intrinsic firing properties of neurons, and may thereby change the configuration of larger functional circuits. The primate orbitofrontal cortex (OFC) receives dopaminergic input from midbrain nuclei, but the role of dopamine in the OFC is still unclear. Here we tested the idea that dopaminergic activity changes the pattern of connectivity between the OFC and the rest of the brain, and thereby reconfigures functional networks in the OFC. To this end, we combined double-blind, placebo-controlled pharmacology (D2 receptor [D2R] antagonist amisulpride) in humans with resting-state functional magnetic resonance imaging (fMRI) and clustering methods. In the placebo group, we replicated previously observed parcellations of the OFC into two and six subregions based on connectivity patterns with the rest of the brain. Most importantly, while the 2-fold clustering did not differ significantly between groups, blocking D2R receptors significantly changed the composition of the 6-fold parcellation, suggesting a dopamine-dependent reconfiguration of functional OFC subregions. Moreover, multivariate decoding analyses revealed that amisulpride changed the whole-brain connectivity patterns of individual OFC-subregions. In particular, D2R blockade shifted the balance of OFC connectivity from associative areas in the temporal and parietal lobe toward functional connectivity with the frontal cortex. In summary, our results suggest that dopamine alters the composition of functional OFC circuits, possibly indicating a broader role for neuromodulators in the dynamic reconfiguration of functional brain networks. **SIGNIFICANCE STATEMENT:** A key role of any neuromodulator may be the reconfiguration of functional brain circuits. Here we test this idea with regard to dopamine and the organization of functional networks in the OFC. We show that blockade of dopamine D2-receptors has profound effects on the functional connectivity patterns of the OFC, yielding in altered connectivity-based subdivisions of this region. Our results suggest that dopamine changes the connectional configuration of the OFC, possibly leading to transitions between different operating modes that favor either sensory input or recurrent processing in the prefrontal cortex. More generally, our findings support a broader role for neuromodulators in the dynamic reconfiguration of functional brain networks and may have clinical implications for understanding the actions of antipsychotics.

DOI: <https://doi.org/10.1523/JNEUROSCI.2827-16.2016>

Posted at the Zurich Open Repository and Archive, University of Zurich

ZORA URL: <https://doi.org/10.5167/uzh-132178>

Journal Article

Accepted Version



The following work is licensed under a Creative Commons: Attribution 4.0 International (CC BY 4.0) License.

Originally published at:

Kahnt, Thorsten; Tobler, Philippe N (2017). Dopamine modulates the functional organization of the orbitofrontal cortex. *Journal of Neuroscience*, 37(6):1493-1504.

DOI: <https://doi.org/10.1523/JNEUROSCI.2827-16.2016>

Research Articles: Behavioral/Cognitive

Dopamine modulates the functional organization of the orbitofrontal cortex

Thorsten Kahnt¹ and Philippe N. Tobler²

¹Department of Neurology, Northwestern University Feinberg School of Medicine, Chicago, IL, 60611, USA

²Department of Economics, Laboratory for Social and Neural Systems Research, University of Zurich, Zürich, 8006, Switzerland

DOI: 10.1523/JNEUROSCI.2827-16.2016

Received: 8 September 2016

Revised: 18 November 2016

Accepted: 28 December 2016

Published: 9 January 2017

Author contributions: T.K. and P.T. designed research; T.K. performed research; T.K. analyzed data; T.K. and P.T. wrote the paper.

Conflict of Interest: The authors declare no competing financial interests.

. Research reported in this publication was supported by the NIDCD of the NIH under Award Number R01DC015426 (to T.K.) and by Swiss National Science Foundation Grants PP00P1_128574, PP00P1_150739, CRSII3_141965, and 00014_165884 (to P.N.T.). The content is solely the responsibility of the authors and does not necessarily represent the official views of the NIH. The authors thank H. Haker, T. Baumgartner, S. Weber, and M. Wälti for assistance in subject recruitment and data acquisition, and M. Mesulam, L.J. Chang, and J.D. Howard for helpful discussions, comments and suggestions.

Correspondence should be addressed to Thorsten Kahnt, Northwestern University, Feinberg School of Medicine, Department of Neurology, 303 E Chicago Ave, Ward 13-006, Chicago, IL 60611, USA. E-Mail: thorsten.kahnt@northwestern.edu

Cite as: J. Neurosci 2017; 10.1523/JNEUROSCI.2827-16.2016

Alerts: Sign up at www.jneurosci.org/cgi/alerts to receive customized email alerts when the fully formatted version of this article is published.

1 Behavioral/Cognitive Section

2

3 Dopamine modulates the functional organization of the orbitofrontal cortex

4

5

6 Thorsten Kahnt^{1*} & Philippe N. Tobler²

7 ¹*Department of Neurology, Northwestern University Feinberg School of Medicine, Chicago, IL, 60611, USA*

8 ²*Department of Economics, Laboratory for Social and Neural Systems Research, University of Zurich, Zürich, 8006,*
9 *Switzerland*

10

11 **Abbreviated title:** Reconfiguration of OFC networks by dopamine

12

13 Number of pages (21)

14 Number of figures (6) and tables (2)

15 Number of words for Abstract (227), Introduction (533), Discussion (1497)

16

17

18 ***Correspondence** should be addressed to Thorsten Kahnt, Northwestern University, Feinberg School of
19 Medicine, Department of Neurology, 303 E Chicago Ave, Ward 13-006, Chicago, IL 60611, USA. E-Mail:
20 thorsten.kahnt@northwestern.edu

21

22

23 **Acknowledgements.** Research reported in this publication was supported by the NIDCD of the NIH under Award
24 Number R01DC015426 (to T.K.) and by Swiss National Science Foundation Grants PP00P1_128574,
25 PP00P1_150739, CRSII3_141965, and 00014_165884 (to P.N.T.). The content is solely the responsibility of the
26 authors and does not necessarily represent the official views of the NIH. The authors thank H. Haker, T.
27 Baumgartner, S. Weber, and M. Wälti for assistance in subject recruitment and data acquisition, and M. Mesulam,
28 L.J. Chang, and J.D. Howard for helpful discussions, comments and suggestions.

29

30 **Conflict of Interest.** The authors declare no competing financial interests.

Abstract

Neuromodulators such as dopamine can alter the intrinsic firing properties of neurons, and may thereby change the configuration of larger functional circuits. The primate orbitofrontal cortex (OFC) receives dopaminergic input from midbrain nuclei, but the role of dopamine in the OFC is still unclear. Here we tested the idea that dopaminergic activity changes the pattern of connectivity between the OFC and the rest of the brain, and thereby reconfigures functional networks in the OFC. To this end, we combined double-blind, placebo-controlled pharmacology (D2 receptor [D2R] antagonist amisulpride) in humans with resting-state functional magnetic resonance imaging (fMRI) and clustering methods. In the placebo group, we replicated previously observed parcellations of the OFC into two and six subregions based on connectivity patterns with the rest of the brain. Most importantly, while the 2-fold clustering did not differ significantly between groups, blocking D2R receptors significantly changed the composition of the 6-fold parcellation, suggesting a dopamine-dependent reconfiguration of functional OFC subregions. Moreover, multivariate decoding analyses revealed that amisulpride changed the whole-brain connectivity patterns of individual OFC-subregions. In particular, D2R blockade shifted the balance of OFC connectivity from associative areas in the temporal and parietal lobe toward functional connectivity with the frontal cortex. In summary, our results suggest that dopamine alters the composition of functional OFC circuits, possibly indicating a broader role for neuromodulators in the dynamic reconfiguration of functional brain networks.

Significance Statement

A key role of any neuromodulator may be the reconfiguration of functional brain circuits. Here we test this idea with regard to dopamine and the organization of functional networks in the OFC. We show that blockade of dopamine D2-receptors has profound effects on the functional connectivity patterns of the OFC, yielding in altered connectivity-based subdivisions of this region. Our results suggest that dopamine changes the connectional configuration of the OFC, possibly leading to transitions between different operating modes that favor either sensory input or recurrent processing in the prefrontal cortex. More generally, our findings support a broader role for neuromodulators in the dynamic reconfiguration of functional brain networks and may have clinical implications for understanding the actions of antipsychotics.

59 Introduction

60 A key function of any neuromodulator may be to alter the dynamics and composition of functional brain circuits
 61 (Marder, 2012). By changing the intrinsic properties of neurons, neuromodulators can differentially affect the
 62 strength of individual synapses, and may thereby bias neurons to transition between, and participate in, different
 63 functional circuits (Harris-Warrick and Marder, 1991; Weimann and Marder, 1994). Importantly, such network
 64 reconfigurations should be reflected in the functional connectivity profile of the brain regions hosting the
 65 functional circuit.

66 The orbitofrontal cortex (OFC) is one of the most connected regions of the brain and participates in several
 67 functional circuits (Kringelbach and Rolls, 2004; Zald and Rauch, 2008). It receives highly processed input from
 68 every sense, and is connected to other prefrontal areas, premotor cortex, and subcortical areas such as the
 69 striatum, amygdala, hippocampus and hypothalamus (Morecraft et al., 1992; Cavada et al., 2000). This dense
 70 connectome suggests that functional interactions with other brain regions are key to the processes that are carried
 71 out by the OFC.

72 Important progress has been made in understanding how the OFC contributes to reward expectation,
 73 valuation, and decision-making (Sescousse et al., 2010; Padoa-Schioppa, 2011; Rushworth et al., 2012; Rudebeck
 74 and Murray, 2014; Howard et al., 2015; Stalnaker et al., 2015). However, although the frontal lobes receive
 75 strong projections from dopaminergic (DA) neurons in the midbrain (Swanson, 1982; Goldman-Rakic et al.,
 76 1992), and DA in the prefrontal cortex (PFC) has been associated with specific cognitive functions such as
 77 working memory and cognitive control (Miller and Cohen, 2001; Cools, 2016), characterizations of the role of
 78 DA in the OFC have remained relatively vague. Specifically, DA in the OFC has been linked to associative
 79 reward processing (Walker et al., 2009), reward-related instrumental behavior (Cetin et al., 2004), and even more
 80 generally, to attention, motivation, and impulsive responding (Winstanley et al., 2010). Interestingly, systemic
 81 modulations of DA have been shown to alter long-range functional connections (Nagano-Saito et al., 2008; Cole
 82 et al., 2013a; Cole et al., 2013b), and DA in the OFC has been linked to dopaminergic neurotransmission in the
 83 striatum (Clarke et al., 2014), suggesting that DA may alter the functional connectivity between the OFC and
 84 remote brain regions.

85 Here we tested the idea that DA modulates the configuration of functional OFC networks. To this end, we
 86 combined DA pharmacology (using the specific D2/D3 receptor [D2R] antagonist amisulpride) with resting-state
 87 functional magnetic resonance imaging (fMRI) and connectivity-based clustering approaches. We parcellated the
 88 OFC into homogeneous subregions based on their functional connectivity patterns with the rest of the brain. In
 89 the placebo group, we replicated a previously observed parcellation into two and six subdivisions (Kahnt et al.,
 90 2012). Importantly, while the 2-fold clustering did not differ between groups, the 6-fold parcellation differed

significantly between groups, suggesting that blocking D2R reconfigured functional networks in the OFC. Moreover, multivariate decoding analyses revealed that whole-brain connectivity patterns of individual OFC subregions were modulated by amisulpride, such that functional connectivity with frontal cortex was enhanced, whereas connections with higher sensory areas were reduced by D2R blockade. These results suggest that monoamines play an important role for the composition of functional OFC circuits, possibly indicating a broader role of neuromodulators in the dynamic reconfiguration of functional brain networks.

Materials and Methods

Participants

A total of 78 healthy male subjects (mean \pm SEM, 22.56 ± 0.27 years) participated in a resting-state fMRI session. Subjects received no visual stimulation and were asked to rest but to stay awake during the 6 minutes of scanning. One and a half hours before the start of the resting-state scan (mean 97.5 ± 0.35 minutes), subjects either received a pill containing placebo ($n = 53$) or 400 mg of the D2R blocker amisulpride ($n = 25$), in a double-blind, pseudorandomized fashion (ratio placebo to amisulpride, 2:1). Groups did not differ significantly in age (placebo: 22.62 ± 0.05 years; amisulpride: 22.52 ± 0.08 years; $t_{76} = 0.18$, $p = 0.86$), weight (placebo = 75.06 ± 0.21 kg; amisulpride: 75.08 ± 0.36 kg; $t_{76} = -0.01$, $p = 0.99$), and subjects were not aware of whether they received placebo or amisulpride, as assessed by a post experimental questionnaire ($\chi^2 = 0.001$, $p = 0.99$). The study was approved by the Cantonal Ethics Review Board of Zurich, and subjects provided informed consent to participate.

fMRI acquisition

Functional imaging was performed on a Philips Achieva 3 T scanner equipped with an eight-channel head coil. A total of 180 T2*-weighted whole-brain echo-planar images (EPI) with 37 transverse slices were acquired with a repetition time (TR) of 2000 ms. Imaging parameters were as follows: slice thickness, 3 mm; in-plane resolution, 2.75×2.75 mm; echo time (TE), 30 ms; flip angle, 90° . Temporal signal-to-noise-ratio (tSNR) in the OFC did not differ between groups ($t_{76} = -1.07$, $p = 0.28$). For normalization purposes, a T1-weighted high-resolution (1×1 mm) structural image was acquired using the following imaging parameters: matrix size, 256×256 ; field of view, 256; 181 slices; flip angle, 8° ; TR = 8.2 ms; TE = 3.8 ms.

120 *Preprocessing of fMRI images*

121 Preprocessing of functional images was performed using SPM12 (Wellcome Department of Imaging
122 Neuroscience, Institute of Neurology, London, UK) and consisted of slice-time correction, realignment, and
123 coregistration of structural and functional images. Spatial normalization to the standard template of the Montreal
124 Neurological Institute (MNI) was performed by estimating deformation fields based on the anatomical image.
125 Deformation fields were used to write two sets of normalized functional images: one with a voxel size of 4 x 4 x 4
126 mm (4 mm set) and one with a voxel size of 3 x 3 x 3 mm (3 mm set). Both sets were spatially smoothed with a
127 Gaussian kernel of 6 mm full width at half maximum (FWHM).

128
129 *Filtering of fMRI time series*

130 Individual fMRI time series were filtered (Fox et al., 2009; Van Dijk et al., 2010) using a general linear model
131 (GLM). The GLM contained: (1-6) six regressors related to between-scan head movements from the realignment
132 procedure, (7) a constant term, (8) a linear trend, (9) the average signal from a white-matter mask, (10) the
133 average signal from a CSF mask, and (11) the average signal from a gray-matter mask. The time-series in each
134 voxel was predicted using this set of 11 regressors and the resulting residuals were high-pass filtered (cutoff = 128
135 s) and used for all subsequent analyses.

136
137 *Orbitofrontal cortex and rest-of-brain mask*

138 The OFC mask was defined using the following AAL map labels: Left and right superior orbital gyrus (2111,
139 2112), left and right middle orbital gyrus (2211, 2212), left and right inferior orbital gyrus (2321, 2322), left and
140 right medial orbital gyrus (2611, 2612), and left and right rectal gyrus (2701, 2702). The resulting OFC mask
141 combined voxels in the left and right medial and lateral orbitofrontal cortex. This OFC mask was subtracted from
142 a whole-brain gray-matter mask, and the resulting voxels were defined as the rest-of-brain mask. Thus, there was
143 no overlap between the rest-of-brain mask and the OFC mask.

144
145 *Connectivity-based parcellation*

146 We subdivided the OFC using a previously published method (Kahnt et al., 2012). In brief, for each OFC voxel,
147 the time-series correlation with every other voxel in the rest-of-brain mask was computed. The resulting

connectivity vectors (one per OFC voxel) were then used to group together OFC voxels that have a similar connectivity profile with the rest of the brain. Similar methods have been used to subdivide brain regions using different measures of connectivity such as diffusion tractography (Johansen-Berg et al., 2004) resting-state fMRI (Kelly et al., 2010) and co-activations (Eickhoff et al., 2011).

We first computed the Pearson correlation coefficient between the time-series in each OFC voxel (from the 3 mm set) and the time-series in every other voxel in the rest-of-brain mask (from the 4 mm set) for each subject. Different voxel sizes were used to maintain high spatial resolution in the OFC while accommodating computational and memory limitations. This resulted in a 2-D correlation matrix ($N = 2771$ OFC by $M = 12,724$ rest-of-brain voxels), where each row reflects the 1-by- M whole-brain connectivity pattern of one OFC voxel. Importantly, because voxels were in MNI space, each voxel has approximately the same anatomical position across subjects allowing averaging of connectivity matrices. Accordingly, individual matrices were averaged across subjects after transforming the correlation coefficients into Fisher's Z scores. The resulting N -by- M matrix was back-transformed into Pearson correlation coefficients and contained the average whole-brain connectivity patterns of all OFC voxels.

The parcellation was performed using the K -means clustering algorithm (*kmeans* as implemented in MATLAB, using the 'correlation' option, i.e. one minus the correlation between the connectivity patterns of OFC voxels as distance measure). Based on our previous study (Kahnt et al., 2012), we computed cluster solutions with $K = 2$ (K2) and $K = 6$ (K6) clusters. For each K , the parcellation was performed 3 times: once for the placebo group, once for the amisulpride group, and once for all subjects together (using a weighted average to account for the unequal group sizes). The parcellation was performed for all voxels in both hemispheres simultaneously. That is, for each K , the connectivity patterns from all OFC voxels were subjected to a single parcellation, irrespective of the anatomical position (i.e. hemisphere) of a given voxel. For each K , we used the best solution from 100 repetitions with different initial centroids.

Note that the nominal labels assigned to the clusters are arbitrary and do not measure anything beyond cluster *identity*. To aid visual inspection and visual comparison between group-wise parcellations, and as requirement for comparing the number of voxels per cluster between groups, the group-wise parcellations were re-labeled to objectively match a template labeling scheme taken from our previous study (Kahnt et al., 2012). For this, we permuted all $K!$ possible cluster label assignments and counted the number of voxels for which the cluster labels matched the template. We then re-labeled the parcellation with the assignment that maximized this number. Voxel-wise cluster maps in MNI space can be obtained from the corresponding author.

180 *Between-group comparison of parcellations*

181 We compared the parcellations between the placebo and amisulpride group using the variation of information (*VI*)
 182 metric (Meila, 2007), which has previously been applied to fMRI connectivity-based parcellations (Kelly et al.,
 183 2010; Kahnt et al., 2012). The *VI* metric is based on mutual information and measures the distance between two
 184 cluster solutions (*C* and *C'*):

$$VI(C, C') = H(C) + H(C') - 2 I(C, C')$$

185 where $H(C)$ and $H(C')$ are the entropies of cluster solutions *C* and *C'*, respectively, and $I(C, C')$ is the mutual
 186 information between *C* and *C'*. $H(C)$ and $I(C, C')$ are computed according to:

$$I(C, C') = \sum_{k=1}^K \sum_{k'=1}^{K'} P(k, k') \log \left(\frac{P(k, k')}{P(k) P(k')} \right)$$

$$H(C) = - \sum_{k=1}^K P(k) \log(P(k))$$

187 $P(k)$ is the probability that a voxel in cluster solution *K* belongs to cluster *k* and $P(k, k')$ is the probability that a
 188 voxel belongs to cluster *k* in *C* and cluster *k'* in *C'*. Following (Meila, 2007), $P(k)$ and $P(k, k')$ are computed
 189 according to:

$$P(k) = \frac{n_k}{n}$$

$$P(k, k') = \frac{|C_k \cap C'_{k'}|}{n}$$

190 where n_k is the number of voxels in cluster *k* and *n* is the total number of OFC voxels. Low values of *VI* indicate
 191 high similarity between the two cluster solutions, whereas high *VI* values indicate large differences.

192 For statistical inference, we employed a permutation test using the parcellations obtained from $n = 1000$
 193 random group assignments. We compared the *VI* of the two empirical group-wise parcellations with the
 194 distribution of *VI*'s of pairs of parcellations obtained from randomly assigned groups. For each permutation, we
 195 randomly assigned subjects to two groups (keeping the original group sizes), computed the group-wise
 196 parcellations for these new groups, and computed the *VI* between the two parcellations. The empirically observed
 197 *VI* was considered significant if larger *VI* values were found in less than 5% of the 1000 random parcellation pairs
 198 ($p < 0.05$).

199

200

201 *Hemispheric Symmetry*

202 To quantify the hemispheric symmetry of the obtained parcellations, we computed a symmetry index *SI* (Kahnt et
 203 al., 2012). This measure reflects the overlap in cluster labels between hemispheres, if one hemisphere is mirrored
 204 at the midline:

$$SI = \frac{1}{N} \sum_i^N \begin{cases} 1 & \text{if } x_i = x'_i \\ 0 & \text{otherwise} \end{cases}$$

205 where *N* is the number of voxels in one hemisphere and *x* and *x'* are the cluster labels of voxel *i* in the original and
 206 mirrored parcellation, respectively. Because this measure requires that each voxel exists in both hemispheres, we
 207 only included voxels that are present in both hemispheres and discarded all voxels that are present on one side
 208 only. Differences in hemispheric symmetry were compared between groups and statistical inference was
 209 performed using a permutation test with *n* = 1000 random group assignments (see *Between-group comparison of*
 210 *parcellations*).

211

212 *Connectivity-based decoding of drug condition*

213 In order to test whether D2R blockade altered the functional connectivity profile of OFC subregions, we used a
 214 between-subject multivariate decoding approach. We aimed to decode the drug condition (amisulpride vs.
 215 placebo) based on the whole-brain connectivity patterns of individual OFC subregions in the K2 and K6
 216 parcellations. To avoid biases, we used the K2 and K6 parcellations computed from all subjects. In contrast to
 217 conventional MVPA approaches that utilize multi-voxel patterns of activity, here we used multi-voxel patterns of
 218 functional connectivity of individual OFC subregions. For each subject, we computed the functional connectivity
 219 (Pearson correlation) between the time series in each OFC subregion (averaged across voxels) and every other
 220 voxel in the rest-of-brain mask, resulting in two and six 1-by-M connectivity patterns, for K2 and K6,
 221 respectively. For each *k* in *K*, the subject-wise 1-by-M connectivity patterns were mean normalized across voxels
 222 (resulting in zero-mean vectors) and used as feature vectors in a support vector machine (SVM) classifier
 223 (www.csie.ntu.edu.tw/~cjlin/libsvm/) with a linear kernel, and 500 random leave two-subjects-out cross-
 224 validation steps. For each cross-validation step, we randomly drew 25 subjects from each group as training data,
 225 and from this subset randomly designated one subject per group as test data. We then used the training data to
 226 train the SVM to distinguish between subjects from the two groups, based on the whole-brain connectivity pattern
 227 of the *k*-th OFC subregion. The classifier was then tested on the two left out subjects and the procedure was

repeated for the next cross-validation step. Decoding accuracy, i.e., %-correct classification in the test data, was averaged across the 500 cross-validation steps.

For statistical inference, we performed a permutation test ($n = 1000$), in which we compared the empirical decoding accuracy to the distribution of decoding accuracies resulting from random permutations of group labels. Specifically, we repeated the identical 500-step cross-validation procedure described above with the exception that after randomly drawing 25 subjects and assigning two subjects as test data, we randomly shuffled the group labels in the training and the test data. This was repeated 1000 times to generate a distribution of accuracies. The empirically observed decoding accuracy was considered significant if larger decoding accuracies were found in less than 5% of the 1000 random permutations ($p < 0.05$).

Mapping of informative voxels

To illustrate the rest-of-brain voxels for which functional connections with OFC subregions were modulated by DA, we examined the weight vector of the SVM classifier. However, rather than directly using the weight vectors from the SVM decoding (i.e., backward) model, we first constructed an encoding (i.e., forward) model based on these weights according to (Haufe et al., 2014):

$$A = S_x W S_g^{-1}$$

Where W is the weight vector of the SVM decoder, and S_x and S_g are the covariance matrices of the training features and labels, respectively.

In contrast to the weights of backward models, the weights of forward models can be interpreted as reflecting the contribution of individual voxels to the separation between the two groups. We averaged the voxel-wise forward weights across the 500 cross-validation steps and divided each weight average by the corresponding standard deviation. This resulted in Z-scores that, for a given OFC subregion, reflect the contribution of voxel-wise connectivity to the separation between groups. We report connections that exceed a threshold of $p < 0.05$, Bonferroni corrected for the number of rest-of-brain voxels ($Z > 4.47$), and that exceed a cluster extent of 2 voxels. For illustration purposes, we display the connectivity maps at a threshold of $p < 0.001$, uncorrected ($Z > 3.72$) with a cluster size of > 5 voxels.

Results

Connectivity-based parcellation of the OFC

Based on our previous findings (Kahnt et al., 2012), we subdivided the OFC into K2 and K6 subregions by grouping together voxels that have a similar pattern of connectivity with the rest of the brain. In a first step, we focused on the placebo group to reveal the functional organization when neuromodulatory activity is undisturbed. The K2 parcellation separated each hemisphere into a (1) medial and (2) anterior lateral subregion (**Figure 1A**). The ventromedial wall (areas 14m, 10, (Mackey and Petrides, 2010)), the gyrus rectus (areas 11m, 14r, 14c), posterior (13), and posterior lateral areas (area 47/12o) formed a network, whereas the remainder of the OFC, i.e., central (area 11), anterior (area 10), and anterior lateral areas (47/12m) formed another network with cohesive connectivity patterns.

In line with our previous findings (Kahnt et al., 2012), the K6 parcellation revealed a (1) medial, a (2) posterior-medial, a (3) central, and three (4-6) lateral clusters spanning the anterior-posterior gradient (**Figure 2A**). In terms of cytoarchitecture, the medial cluster occupied most of the ventromedial wall (areas 14m, 10, 11m) in addition to a small focal part of the lateral posterior OFC (area 13). The posterior-medial cluster consisted of large parts of the gyrus rectus (area 11m, 14r, 14c), as well as parts of more lateral posterior areas (area 13). Regions at the intersection of the transverse and medial orbital sulcus (area 11) formed a central cluster. Finally, the three lateral clusters occupied the posterior-lateral (area 47/12o), mid-lateral (areas 47/12m), and anterior-lateral (areas 10, 11) surface. Overall, both the K2 and K6 parcellations in the placebo group were highly similar to our previous findings (Kahnt et al., 2012).

273

274 *Dopamine changes the connectivity-based parcellation of the OFC*

We next examined how altering dopaminergic neurotransmission through D2R blockade modulated the connectivity-based parcellations described above. Similar to the placebo group, the K2 solution in the amisulpride group revealed a (1) medial and a (2) anterior-lateral cluster (**Figure 1B**). Compared to the placebo group, the anterior-lateral cluster appeared narrower and more stretched along the anterior-posterior axis, dividing the medial cluster into a medial and posterior-lateral segment. However, despite these qualitative differences, a quantitative statistical comparison of the parcellations between the two groups using the *VI* metric revealed that the differences in the K2 parcellation are within the range of what can be expected by chance ($p = 0.278$; **Figure 1C**). In line with this, there were no significant differences between groups in hemispheric symmetry (placebo, $SI = 0.93$; amisulpride, $SI = 0.84$; $p = 0.08$, permutation test; **Figure 3A**), or cluster sizes ($p = 0.169$; **Figure 3C**). These findings may indicate that the 2-cluster organization of the OFC was not substantially altered by changes in dopaminergic neurotransmission.

In contrast, D2R blockade appeared to have caused more pronounced changes in the K6 parcellation (**Figure 2B**). Indeed, a permutation test using the *VI* metric revealed that the K6 parcellations were significantly

different between the two groups ($p = 0.013$; **Figure 2C**). Qualitatively, while the medial (1) and posterior-medial cluster (2) appeared relatively similar to the placebo group, no clearly defined central cluster (3) could be observed in the amisulpride group. Instead, a fourth cluster was revealed on the lateral surface between the anterior lateral and mid-lateral clusters. In line with this, the number of voxels assigned to the central cluster (3) was significantly larger in the amisulpride compared to the placebo group (amisulpride, $N = 491$; placebo, $N = 234$; $p = 0.004$; **Figure 3D**), while the size of the other clusters did not differ significantly (all $p > 0.235$). In addition, the hemispheric symmetry was significantly larger in the placebo group (placebo, $SI = 0.87$; amisulpride, $SI = 0.69$; $p = 0.009$; **Figure 3B**), suggesting that D2R blockade disturbed the symmetry of the functional OFC networks. Taken together, these results demonstrate that the connectivity-based parcellation of the OFC was changed by D2R blockade, suggesting that DA reconfigures functional OFC networks.

Dopamine alters connectivity patterns of individual OFC subregions

The results reported above suggest that the functional connectivity between individual OFC voxels and the rest of the brain was systematically altered by D2R blockade, indicating a DA-dependent reconfiguration of functional OFC networks. In principle, DA-induced changes in the functional connectivity of the OFC could be localized to specific parts of the brain, or could involve the simultaneous modulation of distributed long-range connections. To directly test for such changes in the connectivity patterns of OFC subregions, we utilized a multivariate decoding approach. Specifically, for each subregion in the K2 and K6 parcellation, we used its whole-brain connectivity pattern to decode whether subjects had received placebo or amisulpride prior to scanning. In order to avoid biases, we used a parcellation that was based on all subjects (**Figure 4A and 4B**; however, comparable results were obtained when using the parcellation based on the placebo group only).

Decoding of group membership from the whole-brain connectivity patterns of both clusters in the K2 parcellation was significantly above chance (medial cluster [1], accuracy = 58.5%, $p < 0.001$; anterior lateral cluster [2], accuracy = 55.2%, $p = 0.001$; **Figure 4C**). In the K6 parcellation, we found that drug condition could be decoded significantly above chance from the connectivity patterns of all but two OFC subregions. Significant decoding accuracies were found in the medial (1, accuracy = 54.8 %, $p = 0.001$), posterior-medial (2, accuracy = 60.2 %, $p < 0.001$), central (3, accuracy = 60.0 %, $p < 0.001$), and anterior-lateral cluster (6, accuracy = 57.6 %, $p < 0.001$). The decoding accuracies in the posterior-lateral (4, accuracy = 50.4%, $p = 0.415$) and mid-lateral cluster (5, accuracy = 51.7%, $p = 0.145$) were not significantly different from chance. In summary, D2R blockade modulated the whole-brain connectivity patterns of medial and central OFC sectors, while leaving connectivity of the posterior-lateral clusters unaffected.

To reveal the brain regions in which the connectivity to individual OFC subregions was modulated by D2R blockade, we used the weights of the SVM classifier to estimate voxel-wise connectivity patterns that distinguished between groups (Haufe et al., 2014). For the K2 parcellation, D2R blockade enhanced connectivity of the medial OFC cluster (1) with the amygdala/hippocampus, the superior frontal gyrus, the anterior cingulate cortex, the posterior insula, and the anterior inferior and middle temporal gyrus (**Figure 5A, Table 1**). Conversely, amisulpride reduced connectivity of the medial OFC cluster with posterior inferior temporal gyrus, fusiform gyrus, precuneus, and inferior and superior parietal lobe. In the anterior-lateral cluster (2), D2R blockade enhanced connectivity with the medial and middle frontal gyrus, and the posterior insula, and reduced connectivity with the midbrain, the fusiform gyrus, the precuneus, and the superior parietal lobe (**Figure 5B, Table 1**).

In the K6 parcellation, D2R blockade enhanced connectivity between the medial OFC cluster (1) and the superior and middle frontal gyrus, the anterior cingulate cortex, and the inferior and middle temporal gyrus. In contrast, subjects in the amisulpride group showed reduced medial OFC connectivity with the fusiform gyrus and superior parietal lobe (**Figure 6A, Table 2**). In turn, D2R blockade enhanced connectivity of the posterior-medial OFC cluster (2) with the left amygdala/hippocampus and the middle frontal gyrus, while connectivity with the anterior insula and the precuneus was reduced (**Figure 6B, Table 2**). For the central cluster (3), D2R blockade enhanced connectivity with the middle temporal lobe and the fusiform gyrus. However, the most profound change was a marked reduction in connectivity to the midbrain and the superior temporal gyrus/posterior insula (**Figure 6C, Table 2**). Finally, for the anterior-lateral OFC cluster (6), D2R blockade enhanced connectivity with lateral and medial areas of the PFC, the anterior cingulate cortex and the middle temporal gyrus. In contrast, amisulpride reduced connectivity of the anterior-lateral OFC with the entorhinal cortex, the posterior hippocampus, and the precuneus (**Figure 6D, Table 2**). We did not examine dopamine-dependent modulation of connectivity in the posterior-lateral (4) and mid-lateral (5) OFC clusters because the decoding analyses reported above indicated that the connectivity patterns of these OFC subregions were not significantly modulated by D2R-blockade.

Discussion

In the current study, we used resting-state fMRI connectivity and *K*-means clustering, and demonstrated that systemic administration of amisulpride, a dopaminergic D2R antagonist, altered the configuration of connectional and presumably functional subregions in the OFC. Moreover, D2R blockade had specific effects on voxel-wise connectivity patterns of individual OFC subregions, as indicated by significant decoding of group membership (amisulpride vs. placebo) from these patterns. Amisulpride decreased the connectivity between OFC and

351 associative parietal and temporal regions, and enhanced connectivity of OFC subregions with the medial and
 352 superior-lateral frontal cortex.

353 Previous studies have examined the effects of dopaminergic neurotransmission on large-scale fMRI
 354 connectivity during rest (Cole et al., 2013a; Cole et al., 2013b) and task performance (Honey et al., 2003;
 355 Nagano-Saito et al., 2008). Results of these earlier studies indicate that DA has profound effects on long-range
 356 connectivity between frontal, parietal and subcortical brain regions. However, these studies compared
 357 connectivity within pre-defined regions of interest or “resting-state networks” (e.g., the so-called “default mode”
 358 network), and were therefore not suitable to examine the effects of DA on the configuration of functional circuits
 359 themselves.

360 In contrast, here we used a data-driven method to define functional OFC subregions based on whole-brain
 361 connectivity patterns of individual OFC voxels. Based on our earlier study (Kahnt et al., 2012), anatomical
 362 tracing work in primates (Carmichael and Price, 1996; Ongur and Price, 2000), and the results of a meta-analytic
 363 connectivity modeling study (Zald et al., 2014), we focused on the parcellations with 2 and 6 subdivisions. The
 364 parcellations obtained in the placebo group were highly similar to those found in our previous study (Kahnt et al.,
 365 2012), whereas the parcellation in the amisulpride group revealed specific changes in the organization of
 366 functional OFC subregions. Specifically, whereas the K2 parcellation did not differ between groups, the
 367 organization of the K6 parcellation differed fundamentally, particularly with regard to the central OFC cluster.
 368 Follow-up analyses indicated that D2R blockade was associated with a marked reduction in the connectivity
 369 between the central OFC and the midbrain, suggesting that relative to other parts of OFC, central OFC receives
 370 the strongest DA projections from the midbrain.

371 While null-results should be interpreted with caution, the absence of significant DA-dependent changes in
 372 the K2 subdivision may imply that this subdivision scheme is not modulated by DA and that DA-dependent
 373 modulations only occur at a finer scale. Subregions in the K2 parcellation are well in line with anatomical
 374 boundaries defined cytoarchitectonically and based on anatomical connections. The medial cluster corresponds to
 375 the agranular and dysgranular (i.e., non-isocortical) part of OFC and receives substantial input from the
 376 hippocampus and the amygdala. In contrast, the lateral-anterior cluster corresponds closely to the granular (i.e.,
 377 isocortical) OFC and receives strong projections from the PFC, the insula, the temporal cortex and the medial
 378 dorsal thalamus (Morecraft et al., 1992). This 2-fold parcellation scheme is also consistent with subdivisions
 379 based on intrinsic anatomical connections of the primate OFC (Carmichael and Price, 1994; Kahnt et al., 2012).
 380 However, although D2R blockade did not alter the outlines of the K2 subdivision, it did modulate the functional
 381 connectivity patterns of these subregions, suggesting that while the configuration of the coarse functional network
 382 was not affected by DA, the specific balance of connections within the network was changed.

383 The reconfiguration observed in the K6 parcellation is likely to be driven by a DA-dependent modulation of
 384 the connections between individual OFC voxels and remote brain regions. At the cellular level, amisulpride acts
 385 as an antagonist on D2 and D3 receptors, and reduces the post-synaptic effects of DA on neurons (Rosenzweig et
 386 al., 2002). In addition, amisulpride blocks presynaptic autoreceptors, effectively increasing the availability of DA
 387 in the synaptic cleft. Accordingly, any combination of pre- and post-synaptic receptor blockade will therefore
 388 increase the ratio of D1 to D2 receptor activation. By modulating the intrinsic firing properties of individual
 389 neurons, DA may change the strength of specific synapses and thereby the connectivity to other neurons,
 390 effectively altering the role of individual neurons in its larger circuit (Kloppenburg et al., 1999; Harris-Warrick
 391 and Johnson, 2010). Such changes are not necessarily binary switches (i.e., on-off) between connections, but
 392 could involve smooth transitions in the composition of interconnected networks. Interestingly, neuromodulator-
 393 induced changes in connectivity may be associated with different modes of operation responsible for different
 394 behaviors (Harris-Warrick and Marder, 1991; Weimann and Marder, 1994). The hard-wired anatomical
 395 connections between brain regions may therefore only provide the structure in which several possible functional
 396 networks, each associated with specific processing modes and behaviors, can be initialized depending on the
 397 current neuromodulatory environment (Brezina, 2010; Marder, 2012).

398 Our results show that connections between individual OFC subregions and higher-order sensory and
 399 multimodal association areas in the parietal and temporal lobes were dampened by D2R blockade. In contrast,
 400 connectivity between the OFC and the medial and superior PFC were upregulated by amisulpride. This suggests
 401 that DA activity on D2R switches the OFC between two distinct connectional configurations that may be
 402 associated with different processing modes. The first configuration, induced by high levels of D2R activity, is
 403 characterized by enhanced connectivity to higher sensory and associative areas, and may help sensory information
 404 to access the OFC. A second configuration, induced by low D2R activity, is characterized by enhanced short-
 405 range functional connections with the frontal lobes, and may facilitate local information processing in the frontal
 406 cortex.

407 This proposal is in line with the effects of receptor-specific DA activity in a biophysically inspired dual-
 408 state model of DA in the PFC (Durstewitz et al., 2000; Seamans et al., 2001). Specifically, in this model, the ratio
 409 of D1 and D2 receptor activity modulates local GABAergic inhibition and thereby controls the balance between
 410 the stability and flexibility of PFC representations. Reduced D2R activity facilitates recurrent excitation in the
 411 network and stabilizing PFC representations, whereas enhanced D2R activity inhibits recurrent excitation and
 412 increases the flexibility of PFC representations (Seamans and Yang, 2004). Supporting this model, we have
 413 previously shown that D2R blockade enhances decoding of reward information from OFC activity patterns,
 414 suggesting that corresponding networks representations were strengthened (Kahnt et al., 2015).

415 Importantly, switches between the two OFC network configurations could be implemented solely by
 416 changes in local DA concentrations. Specifically, DA has a higher affinity for D2 than D1 receptors (Creese et
 417 al., 1983), and therefore low levels of DA may lead to stronger D2 vs. D1 activity, whereas robust activity of D1
 418 receptors is only achieved with high levels of DA (Goto and Grace, 2005). Thus, bursts of DA, like those elicited
 419 by unexpected rewards or reward-predictive stimuli (Schultz et al., 1997; Schultz, 2016), may drive the OFC into
 420 a D1 dominated state with enhanced connectivity to frontal brain regions and reduced connectivity to sensory
 421 areas, promoting local information processing and representational stability. Conversely, low levels of DA, like
 422 those observed when expected rewards are omitted (Bayer and Glimcher, 2005; Takahashi et al., 2009), may
 423 preferentially activate D2 receptors which may reduce connections to the PFC, enhance sensory input to the OFC,
 424 and facilitate reorientation, representational updating and behavioral flexibility. Interestingly, a recent model of
 425 OFC functioning proposes that OFC contributes to goal-directed behavior by representing a cognitive map, or
 426 associative structure, for reinforcement learning (Wilson et al., 2014; Howard et al., 2015; Schuck et al., 2016;
 427 Wikenheiser and Schoenbaum, 2016). Our results indicate that DA may play a critical role in updating of OFC
 428 state-representations.

429 It is important to note that although amisulpride is one of the few relatively selective drugs affecting DA
 430 transmission, it also has high affinity for serotonin receptors 5-HT_{2B} and 5-HT₇. Accordingly, the effects
 431 observed here may not be the result of DA alone. However, insofar as serotonin and DA are both monoamines,
 432 we can conclude that our results are driven by monoaminergic neuromodulators. We also note that connectivity
 433 changes between the OFC and any other brain region may be caused indirectly through connectivity changes
 434 between this region and a third region whose connectivity to OFC is modulated by DA. Thus, OFC connectivity
 435 changes with individual areas need to be interpreted with caution as indirect modulations cannot be ruled out.
 436 Finally, in the current study, we examined the effects of D2R blockade on connectivity during rest. It is possible
 437 that OFC networks are differentially modulated during performance of specific tasks. Functional connectivity
 438 between areas partially depends on task-dependent activity levels which may result in different parcellation
 439 schemes. Future studies are needed to examine OFC network configurations as a function of different tasks.

440 In summary, here we have shown that D2R blockade changes the functional organization of the OFC. We
 441 speculate that midbrain DA may alter the connectional configuration of the OFC, leading to transitions between
 442 different operating modes that favor either sensory input or recurrent processing. Finally, the results obtained
 443 here for DA could exemplify a more general role of neuromodulators in altering the connectivity patterns of brain
 444 regions. This change in connectivity may lead to the reconfiguration of specific functional circuits that may be
 445 associated with different modes of information processing and ultimately distinct behaviors.

446 **References**

- 447 Bayer HM, Glimcher PW (2005) Midbrain dopamine neurons encode a quantitative reward prediction error
448 signal. *Neuron* 47:129-141.
- 449 Brezina V (2010) Beyond the wiring diagram: signalling through complex neuromodulator networks. *Philos*
450 *Trans R Soc Lond B Biol Sci* 365:2363-2374.
- 451 Carmichael ST, Price JL (1994) Architectonic Subdivision of the Orbital and Medial Prefrontal Cortex in the
452 Macaque Monkey. *Journal of Comparative Neurology* 346:366-402.
- 453 Carmichael ST, Price JL (1996) Connectional networks within the orbital and medial prefrontal cortex of
454 macaque monkeys. *J Comp Neurol* 371:179-207.
- 455 Cavada C, Company T, Tejedor J, Cruz-Rizzolo RJ, Reinoso-Suarez F (2000) The anatomical connections of the
456 macaque monkey orbitofrontal cortex. A review. *Cereb Cortex* 10:220-242.
- 457 Cetin T, Freudenberg F, Fuchtemeier M, Koch M (2004) Dopamine in the orbitofrontal cortex regulates operant
458 responding under a progressive ratio of reinforcement in rats. *Neurosci Lett* 370:114-117.
- 459 Clarke HF, Cardinal RN, Rygula R, Hong YT, Fryer TD, Sawiak SJ, Ferrari V, Cockcroft G, Aigbirhio FI,
460 Robbins TW, Roberts AC (2014) Orbitofrontal dopamine depletion upregulates caudate dopamine and
461 alters behavior via changes in reinforcement sensitivity. *J Neurosci* 34:7663-7676.
- 462 Cole DM, Beckmann CF, Oei NY, Both S, van Gerven JM, Rombouts SA (2013a) Differential and distributed
463 effects of dopamine neuromodulations on resting-state network connectivity. *Neuroimage* 78:59-67.
- 464 Cole DM, Oei NY, Soeter RP, Both S, van Gerven JM, Rombouts SA, Beckmann CF (2013b) Dopamine-
465 dependent architecture of cortico-subcortical network connectivity. *Cereb Cortex* 23:1509-1516.
- 466 Cools R (2016) The costs and benefits of brain dopamine for cognitive control. *Wiley Interdiscip Rev Cogn Sci*
467 7:317-329.
- 468 Creese I, Sibley DR, Hamblin MW, Leff SE (1983) The classification of dopamine receptors: relationship to
469 radioligand binding. *Annu Rev Neurosci* 6:43-71.
- 470 Durstewitz D, Seamans JK, Sejnowski TJ (2000) Dopamine-mediated stabilization of delay-period activity in a
471 network model of prefrontal cortex. *J Neurophysiol* 83:1733-1750.
- 472 Eickhoff SB, Bzdok D, Laird AR, Roski C, Caspers S, Zilles K, Fox PT (2011) Co-activation patterns distinguish
473 cortical modules, their connectivity and functional differentiation. *Neuroimage* 57:938-949.
- 474 Fox MD, Zhang D, Snyder AZ, Raichle ME (2009) The global signal and observed anticorrelated resting state
475 brain networks. *J Neurophysiol* 101:3270-3283.
- 476 Goldman-Rakic PS, Lidow MS, Smiley JF, Williams MS (1992) The anatomy of dopamine in monkey and human
477 prefrontal cortex. *J Neural Transm Suppl* 36:163-177.
- 478 Goto Y, Grace AA (2005) Dopaminergic modulation of limbic and cortical drive of nucleus accumbens in goal-
479 directed behavior. *Nat Neurosci* 8:805-812.
- 480 Harris-Warrick RM, Marder E (1991) Modulation of neural networks for behavior. *Annu Rev Neurosci* 14:39-57.
- 481 Harris-Warrick RM, Johnson BR (2010) Checks and balances in neuromodulation. *Front Behav Neurosci* 4.
- 482 Haufe S, Meinecke F, Gorgen K, Dahne S, Haynes JD, Blankertz B, Biessmann F (2014) On the interpretation of
483 weight vectors of linear models in multivariate neuroimaging. *Neuroimage* 87:96-110.
- 484 Honey GD, Suckling J, Zelaya F, Long C, Routledge C, Jackson S, Ng V, Fletcher PC, Williams SC, Brown J,
485 Bullmore ET (2003) Dopaminergic drug effects on physiological connectivity in a human cortico-striato-
486 thalamic system. *Brain* 126:1767-1781.
- 487 Howard JD, Gottfried JA, Tobler PN, Kahnt T (2015) Identity-specific coding of future rewards in the human
488 orbitofrontal cortex. *Proc Natl Acad Sci U S A* 112:5195-5200.
- 489 Johansen-Berg H, Behrens TE, Robson MD, Drobniak I, Rushworth MF, Brady JM, Smith SM, Higham DJ,
490 Matthews PM (2004) Changes in connectivity profiles define functionally distinct regions in human
491 medial frontal cortex. *Proc Natl Acad Sci U S A* 101:13335-13340.
- 492 Kahnt T, Chang LJ, Park SQ, Heinze J, Haynes JD (2012) Connectivity-based parcellation of the human
493 orbitofrontal cortex. *J Neurosci* 32:6240-6250.
- 494 Kahnt T, Weber SC, Haker H, Robbins TW, Tobler PN (2015) Dopamine D2-receptor blockade enhances
495 decoding of prefrontal signals in humans. *J Neurosci* 35:4104-4111.

- 496 Kelly C, Uddin LQ, Shehzad Z, Margulies DS, Castellanos FX, Milham MP, Petrides M (2010) Broca's region:
497 linking human brain functional connectivity data and non-human primate tracing anatomy studies. *Eur J*
498 *Neurosci* 32:383-398.
- 499 Kloppenburg P, Levini RM, Harris-Warrick RM (1999) Dopamine modulates two potassium currents and inhibits
500 the intrinsic firing properties of an identified motor neuron in a central pattern generator network. *J*
501 *Neurophysiol* 81:29-38.
- 502 Kringelbach ML, Rolls ET (2004) The functional neuroanatomy of the human orbitofrontal cortex: evidence from
503 neuroimaging and neuropsychology. *Prog Neurobiol* 72:341-372.
- 504 Mackey S, Petrides M (2010) Quantitative demonstration of comparable architectonic areas within the
505 ventromedial and lateral orbital frontal cortex in the human and the macaque monkey brains. *Eur J*
506 *Neurosci* 32:1940-1950.
- 507 Marder E (2012) Neuromodulation of neuronal circuits: back to the future. *Neuron* 76:1-11.
- 508 Meila M (2007) Comparing clusterings - an information based distance. *J Multivariate Anal* 98:873-895.
- 509 Miller EK, Cohen JD (2001) An integrative theory of prefrontal cortex function. *Annu Rev Neurosci* 24:167-202.
- 510 Morecraft RJ, Geula C, Mesulam MM (1992) Cytoarchitecture and neural afferents of orbitofrontal cortex in the
511 brain of the monkey. *J Comp Neurol* 323:341-358.
- 512 Nagano-Saito A, Leyton M, Monchi O, Goldberg YK, He Y, Dagher A (2008) Dopamine depletion impairs
513 frontostriatal functional connectivity during a set-shifting task. *J Neurosci* 28:3697-3706.
- 514 Ongur D, Price JL (2000) The organization of networks within the orbital and medial prefrontal cortex of rats,
515 monkeys and humans. *Cereb Cortex* 10:206-219.
- 516 Padoa-Schioppa C (2011) Neurobiology of economic choice: a good-based model. *Annu Rev Neurosci* 34:333-
517 359.
- 518 Rosenzweig P, Canal M, Patat A, Bergougnan L, Zieleniuk I, Bianchetti G (2002) A review of the
519 pharmacokinetics, tolerability and pharmacodynamics of amisulpride in healthy volunteers. *Hum*
520 *Psychopharmacol* 17:1-13.
- 521 Rudebeck PH, Murray EA (2014) The orbitofrontal oracle: cortical mechanisms for the prediction and evaluation
522 of specific behavioral outcomes. *Neuron* 84:1143-1156.
- 523 Rushworth MF, Kolling N, Sallet J, Mars RB (2012) Valuation and decision-making in frontal cortex: one or
524 many serial or parallel systems? *Curr Opin Neurobiol* 22:946-955.
- 525 Schuck NW, Cai MB, Wilson RC, Niv Y (2016) Human Orbitofrontal Cortex Represents a Cognitive Map of
526 State Space. *Neuron* 91:1402-1412.
- 527 Schultz W (2016) Dopamine reward prediction-error signalling: a two-component response. *Nat Rev Neurosci*
528 17:183-195.
- 529 Schultz W, Dayan P, Montague PR (1997) A neural substrate of prediction and reward. *Science* 275:1593-1599.
- 530 Seamans JK, Yang CR (2004) The principal features and mechanisms of dopamine modulation in the prefrontal
531 cortex. *Prog Neurobiol* 74:1-58.
- 532 Seamans JK, Gorelova N, Durstewitz D, Yang CR (2001) Bidirectional dopamine modulation of GABAergic
533 inhibition in prefrontal cortical pyramidal neurons. *J Neurosci* 21:3628-3638.
- 534 Sescousse G, Redoute J, Dreher JC (2010) The architecture of reward value coding in the human orbitofrontal
535 cortex. *J Neurosci* 30:13095-13104.
- 536 Stalnaker TA, Cooch NK, Schoenbaum G (2015) What the orbitofrontal cortex does not do. *Nat Neurosci* 18:620-
537 627.
- 538 Swanson LW (1982) The projections of the ventral tegmental area and adjacent regions: a combined fluorescent
539 retrograde tracer and immunofluorescence study in the rat. *Brain Res Bull* 9:321-353.
- 540 Takahashi YK, Roesch MR, Stalnaker TA, Haney RZ, Calu DJ, Taylor AR, Burke KA, Schoenbaum G (2009)
541 The orbitofrontal cortex and ventral tegmental area are necessary for learning from unexpected outcomes.
542 *Neuron* 62:269-280.
- 543 Van Dijk KR, Hedden T, Venkataraman A, Evans KC, Lazar SW, Buckner RL (2010) Intrinsic functional
544 connectivity as a tool for human connectomics: theory, properties, and optimization. *J Neurophysiol*
545 103:297-321.

- Walker SC, Robbins TW, Roberts AC (2009) Differential contributions of dopamine and serotonin to orbitofrontal cortex function in the marmoset. *Cereb Cortex* 19:889-898.
- Weimann JM, Marder E (1994) Switching Neurons Are Integral Members of Multiple Oscillatory Networks. *Current Biology* 4:896-902.
- Wikenheiser AM, Schoenbaum G (2016) Over the river, through the woods: cognitive maps in the hippocampus and orbitofrontal cortex. *Nature reviews Neuroscience* 17:513-523.
- Wilson RC, Takahashi YK, Schoenbaum G, Niv Y (2014) Orbitofrontal cortex as a cognitive map of task space. *Neuron* 81:267-279.
- Winstanley CA, Zeeb FD, Bedard A, Fu K, Lai B, Steele C, Wong AC (2010) Dopaminergic modulation of the orbitofrontal cortex affects attention, motivation and impulsive responding in rats performing the five-choice serial reaction time task. *Behav Brain Res* 210:263-272.
- Zald DH, Rauch SL (2008) *The orbitofrontal cortex*, 1st paperback Edition. Oxford ; New York: Oxford University Press.
- Zald DH, McHugo M, Ray KL, Glahn DC, Eickhoff SB, Laird AR (2014) Meta-analytic connectivity modeling reveals differential functional connectivity of the medial and lateral orbitofrontal cortex. *Cereb Cortex* 24:232-248.

563 **Figure Legends**

564 **Figure 1. Connectivity-based parcellation of the OFC into K2 subregions.** A. 2-fold clustering in the placebo
 565 group. B. 2-fold clustering in the amisulpride group. C. Histogram of variation of information (VI) values
 566 comparing pairs of K2 parcellations from random group assignments. Red vertical line depicts the VI value
 567 comparing the actual group-wise parcellations of the placebo and amisulpride group.

568

569 **Figure 2. Connectivity-based parcellation of the OFC into K6 subregions.** A. 6-fold clustering in the placebo
 570 group. B. 6-fold clustering in the amisulpride group. C. Histogram of VI values comparing pairs of K6
 571 parcellations from random group assignments. Red vertical line depicts the VI value comparing the actual group-
 572 wise parcellations of the placebo and amisulpride group. Asterisk indicates a significant group difference from
 573 chance at $p < 0.05$.

574

575 **Figure 3. Comparison of group-wise parcellations.** A. Histogram of the difference in hemispheric symmetry
 576 between the pairs of K2 parcellations from randomly assigned groups. Red vertical line depicts the empirical
 577 difference in hemispheric symmetry between the placebo and amisulpride group. B. same as in A, but for the K6
 578 parcellation. C. Each histogram depicts the difference in the cluster size (number of voxels) between two groups
 579 randomly assigned groups in cluster 1 (top) and 2 (bottom) of the K2 parcellation. Red vertical lines depict the
 580 empirical difference in cluster size between the placebo and amisulpride group. D. Same as in C, but for the K6
 581 parcellation. Asterisks indicate significant differences from zero at $p < 0.05$.

582

583 **Figure 4. Decoding drug condition from connectivity patterns of individual OFC subregions.** A. K2
 584 parcellation based on all subjects. B. K6 parcellation based on all subjects. C. Decoding accuracy (%-correct
 585 group classifications of placebo vs. amisulpride) for each of the two OFC subregions of the K2 parcellation. D.
 586 Decoding accuracy for each of the six OFC subregions of the K6 parcellation. Error bars indicate 95% CI around
 587 empirical chance-level (~50%) based on 1000 random permutations. Asterisks indicate significant above-chance
 588 classification at $p < 0.05$, corrected.

589

590 **Figure 5. Effects of D2R blockade on voxel-wise OFC-connectivity of K2 subregions.** Maps depict the
 591 contribution of the voxel-wise connectivity of the medial (A) and lateral (B) OFC subregion of the K2
 592 parcellation to the separation between the amisulpride and placebo group. Connectivity patterns are estimated

593 based on SVM weight-vectors and then converted into Z-scores. For illustration purposes, maps are thresholded
594 at $p < 0.001$, uncorrected ($Z > 3.72$) with a voxel extent threshold of 5.

595

596 **Figure 6. Effects of D2R blockade on voxel-wise OFC-connectivity of K6 subregions.** Maps depict the
597 contribution of the voxel-wise connectivity of the medial (**A**), posterior-medial (**B**), central (**C**), and anterior
598 lateral (**D**) OFC subregion of the K6 parcellation to the separation between the amisulpride and placebo group.
599 Connectivity patterns are estimated based on SVM weight-vectors and then converted into Z-scores. For
600 illustration purposes, maps are thresholded at $p < 0.001$, uncorrected ($Z > 3.72$) with a voxel extent threshold of 5.

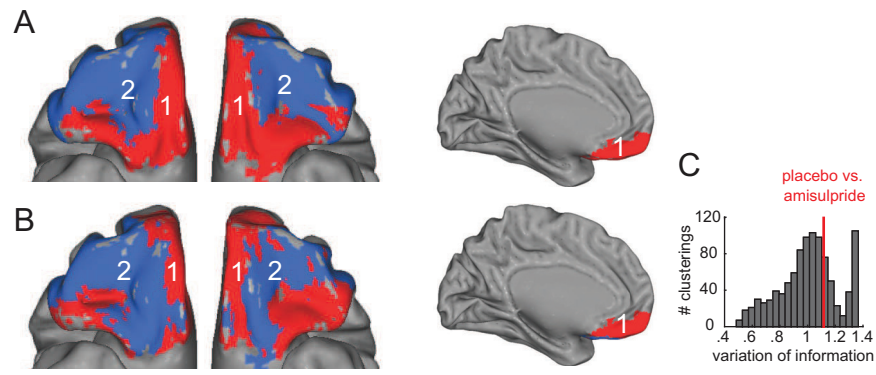
601

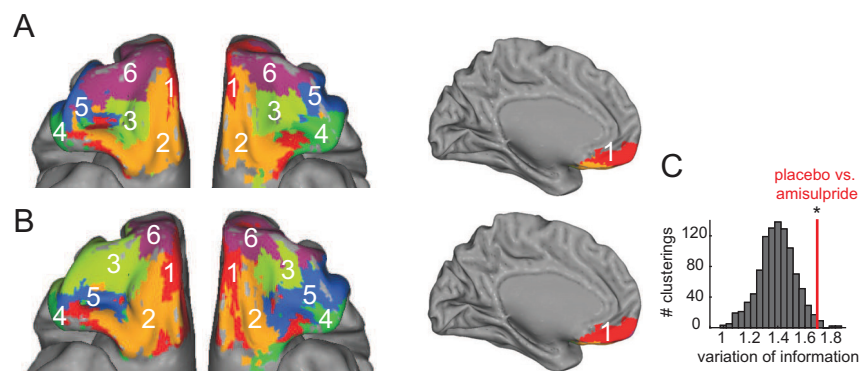
602 **Table Legends**

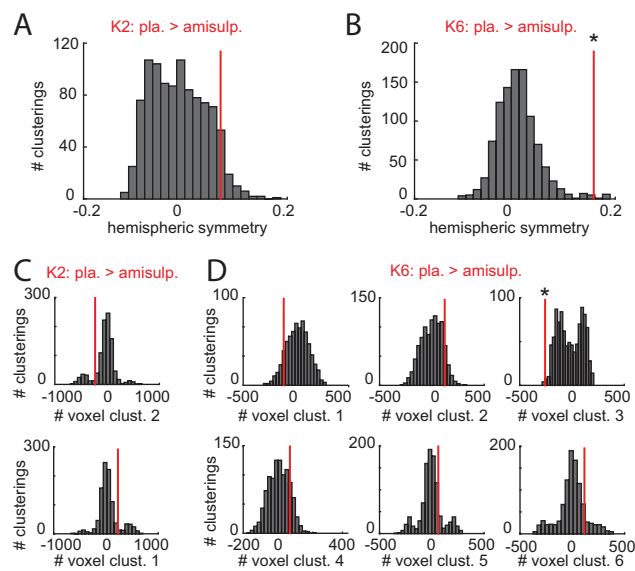
603 **Table 1.** Anatomical labels, MNI coordinates (x, y, z), Z-scores, and cluster size (number of voxels) for whole-
604 brain connectivity of individual OFC subregions in the K2 parcellation contributing to the separation between
605 groups, thresholded at $p < 0.05$, Bonferroni corrected ($Z > 4.47$) and $k > 2$.

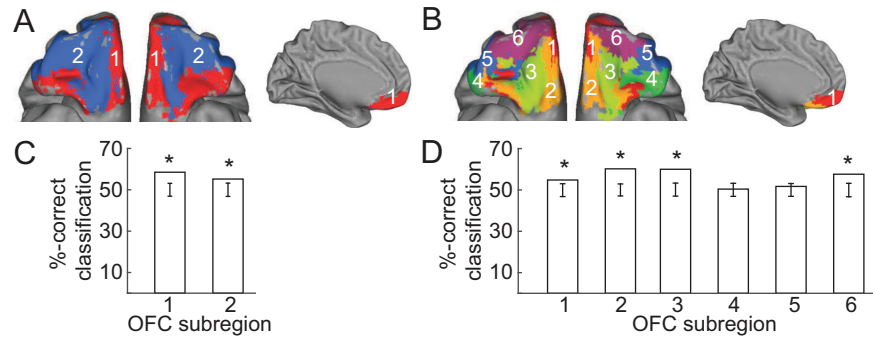
606

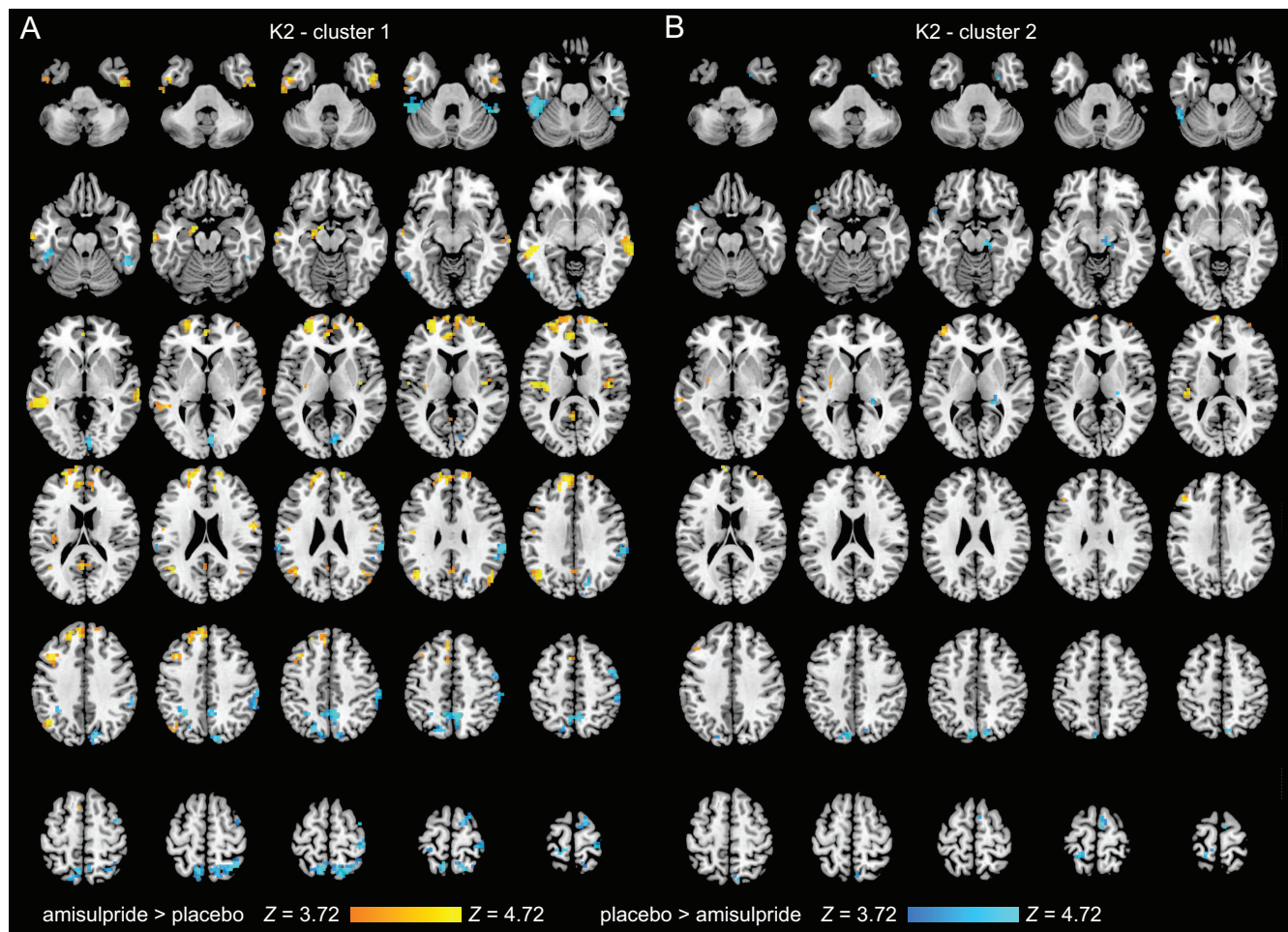
607 **Table 2.** Anatomical labels, MNI coordinates (x, y, z), Z-scores, and cluster size (number of voxels) for whole-
608 brain connectivity of individual OFC subregions in the K6 parcellation contributing to the separation between
609 groups, thresholded at $p < 0.05$, Bonferroni corrected ($Z > 4.47$) and $k > 2$.











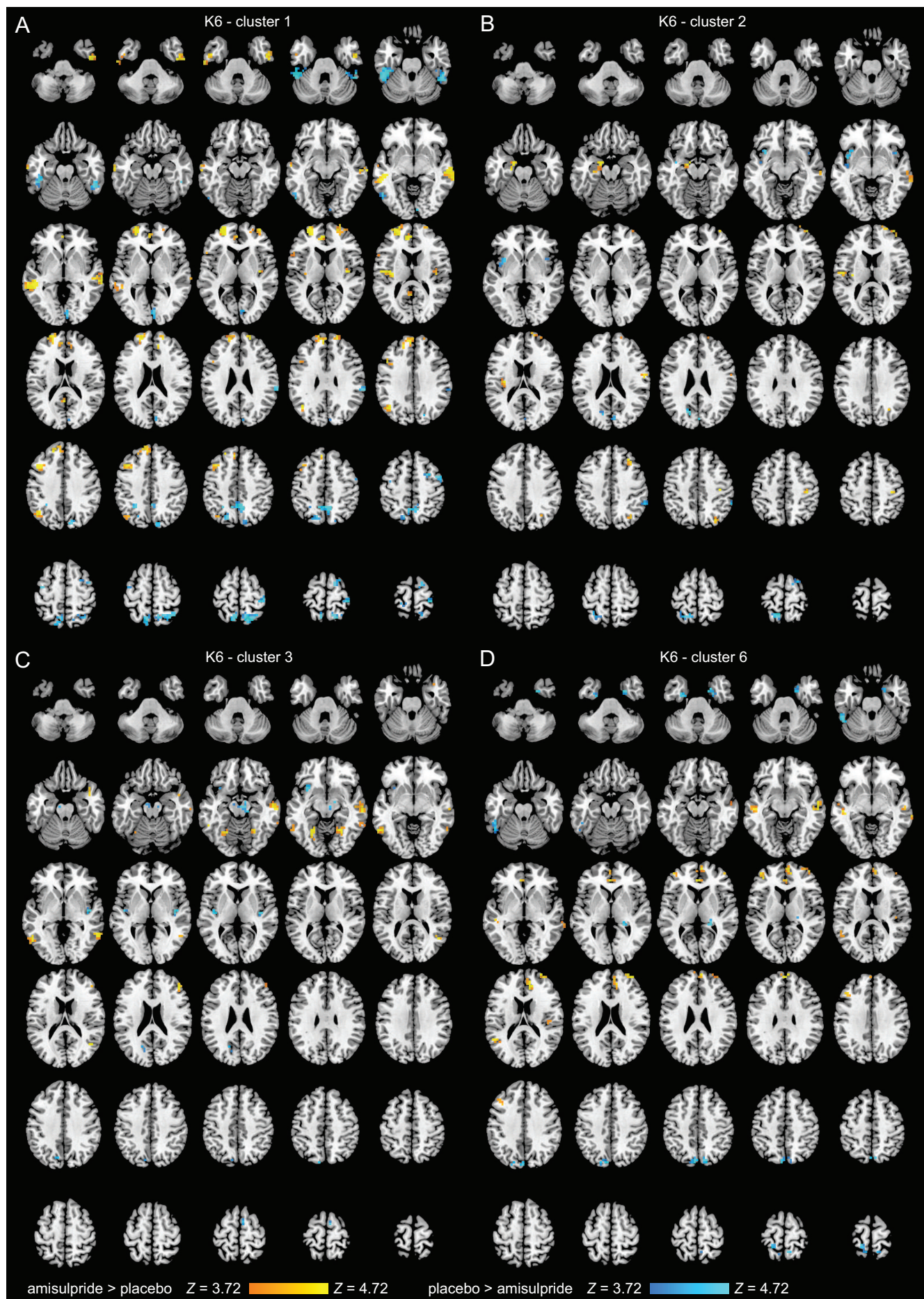


Table 1. Dopamine-dependent connectivity of subregions in the K2 parcellation.

Side	Anatomical label	MNI (x, y, z)			N voxel	Z-score
Cluster 1 - Amisulpride > Placebo						
L	amygdala/hippocampus	-14	-4	-18	5	6.09
L	superior frontal gyrus	-26	56	6	49	6.99
R	superior frontal gyrus	26	68	10	16	5.29
L	anterior cingulate cortex	-6	48	14	14	6.69
L	superior frontal gyrus	-18	44	38	4	5.99
L	middle frontal gyrus	-42	44	38	6	5.02
L	insula	-38	-16	14	12	5.43
R	insula	38	-12	10	5	6.09
L	middle temporal gyrus	-54	-36	-6	22	5.51
R	middle temporal gyrus	70	-32	-6	12	5.45
L	middle temporal gyrus	-66	-16	-22	3	5.33
L	inferior temporal cortex	-50	-4	-34	3	4.83
R	inferior temporal cortex	54	-4	-34	3	5.56
L	precuneus	-2	-52	18	3	5.03
L	inferior parietal lobe	-42	-64	34	17	5.70
Cluster 1 - Placebo > Amisulpride						
R	middle frontal gyrus	42	0	58	3	4.61
R	superior frontal gyrus	14	0	70	3	5.14
R	precentral gyrus	38	-32	66	3	5.48
L	postcentral gyrus	-10	-36	78	5	5.67
L	middle temporal gyrus	-54	-64	-6	3	4.98
L	fusiform gyrus	-50	-44	-26	33	7.17
R	fusiform gyrus	50	-44	-30	14	6.27
L	precuneus	-10	-52	46	36	6.65
R	precuneus	6	-52	46		6.48
R	superior parietal lobe	18	-60	66	21	5.34
L	inferior parietal lobe	-26	-52	42	6	5.96
R	inferior parietal lobe	66	-32	30	15	6.21
R	occipital cortex	2	-84	2	8	5.07
Cluster 3 - Amisulpride > Placebo						
L	medial frontal gyrus	-6	68	14	4	5.43
L	middle frontal gyrus	-42	28	34	3	4.69
L	insula	-46	-24	14	3	4.77
Cluster 2 - Placebo > Amisulpride						
R	midbrain	14	-24	-14	4	6.76
L	Fusiform gyrus	-50	-52	-26	3	4.93
L	precuneus	-6	-80	46	10	5.76
L	superior parietal lobe	-18	-40	74	3	5.02

Table 2. Dopamine-dependent connectivity of subregions in the K6 parcellation.

Side	Region	MNI (x, y, z)			N voxel	Z-score
Cluster 1 - Amisulpride > Placebo						
L	superior frontal gyrus	-26	56	6	42	7.84
L	superior frontal gyrus	-6	52	30	4	5.23
L	superior frontal gyrus	-18	44	38	5	5.16
R	superior frontal gyrus	18	56	26	4	5.11
L	middle frontal gyrus	-42	16	38	10	5.52
L	anterior cingulate cortex	-6	48	14	8	6.67
L	insula	-38	-16	14	8	5.29
R	insula	38	-12	10	3	5.84
L	middle temporal gyrus	-46	-28	-6	22	6.07
R	middle temporal gyrus	66	-28	-2	22	5.34
L	inferior temporal gyrus	-58	-16	-34	3	4.90
R	inferior temporal gyrus	46	-12	-42	14	6.16
L	inferior parietal lobe	-46	-64	38	8	5.13
Cluster 1 - Placebo > Amisulpride						
R	superior frontal gyrus	14	-4	70	3	5.14
R	middle frontal gyrus	46	0	54	3	4.91
L	postcentral gyrus	-10	-40	78	3	4.90
R	postcentral gyrus	38	-32	66	6	5.68
L	inferior temporal gyrus	-50	-40	-26	31	6.94
R	inferior temporal gyrus	50	-48	-26	16	5.75
L	inferior temporal gyrus	-54	-60	-6	3	4.66
R	superior parietal gyrus	18	-60	66	23	6.31
R	precuneus	6	-52	46	28	6.26
L	precuneus	-14	-68	50	4	5.19
L	inferior parietal lobe	-26	-52	42	3	5.29
R	inferior parietal lobe	66	-28	26	5	5.20
R	occipital cortex	6	-80	2	4	4.61
Cluster 2 - Amisulpride > Placebo						
L	amygdala/hippocampus	-18	-4	-18	8	6.32
R	middle frontal gyrus	38	60	14	3	5.12
R	postcentral gyrus	38	-24	50	3	5.22
Cluster 2 - Placebo > Amisulpride						
L	insula	-38	12	-6	3	4.69
L	middle frontal gyrus	-38	0	54	3	4.73
R	superior temporal gyrus	46	-12	-2	3	5.55
L	precuneus	-22	-56	66	7	4.96
L	precuneus	-18	-68	26	3	5.82
Cluster 3 - Amisulpride > Placebo						
R	middle temporal gyrus	58	-12	-14	8	5.11

L	middle temporal gyrus	-54	-60	-2	6	5.46
R	middle temporal gyrus	58	-56	-2	4	5.12
R	middle temporal gyrus	46	-60	18	3	4.88
L	fusiform gyrus	-26	-64	-10	8	5.54
R	fusiform gyrus	26	-56	-10	4	5.14
<i>Cluster 3 - Placebo > Amisulpride</i>						
R	midbrain	10	-16	-14	3	5.10
R	superior temporal gyrus	42	-12	-2	7	5.76
<i>Cluster 6 - Amisulpride > Placebo</i>						
R	superior frontal gyrus	2	56	30	4	5.00
R	medial frontal gyrus	6	60	6	5	4.84
R	anterior cingulate cortex	2	40	6	5	5.07
R	anterior cingulate cortex	10	40	18	6	5.17
R	superior frontal gyrus	30	60	18	5	4.95
L	middle temporal gyrus	-46	-28	-6	4	5.90
R	middle temporal gyrus	58	-16	-10	4	5.48
<i>Cluster 6 - Placebo > Amisulpride</i>						
R	entorhinal cortex	22	0	-38	6	5.52
R	hippocampus	22	-36	6	4	5.13
L	inferior temporal gyrus	-50	-52	-26	4	4.91
L	precuneus	-6	-80	46	5	5.72